Control of grid forming inverter based on robust IDA-PBC for power quality enhancement

Nidhal Khefifi, Azeddine Houari, Mohamed Machmoum, Malek Ghanes, Mourad Aït-Ahmed

Control of Grid Forming Inverter Based on Robust IDA-PBC for Power Quality Enhancement

Nidhal KHEFIFI [1]*, Azeddine HOUARI [1], Mohamed MACHMOUM [1], Malek GHANES [2], Mourad AIT-AHMED [1]

[1] IREENA, University of Nantes, Saint-Nazaire, France.

[2] LS2N, Ecole Centrale de Nantes, Nantes, France

*nidhal.khefifi@etu.univ-nantes.fr

Abstract: This paper deal with power quality issues in weak voltage isolated micro-grids, where the power export is managed through an inverter connected via an LC filter to feed the local consumers. In this context, a robust Interconnection and Damping Assignment Passivity-Based Controller (IDA-PBC) with an integral action is proposed to cope with undesired disturbances and uncertainties. The synthesis methodology of this kind of control is based on Hamiltonian modeling where the objective is to minimize a desired energy function that guarantees a stable and robust control of the system in a closed-loop. The design steps of the proposed control are provided and its effectiveness is shown through comparative experimental tests between a classical PI controller and an IDA-PBC controller.

Index terms- Voltage control; Power quality; standalone micro grid; IDA-PBC control.

1. Introduction

Today's energy transition challenges make the development of Microgrids (MG) as the main solution to integrate sustainable energy systems that meet with numerous environmental, techno-economic, and energy-security requirements[1–3] . These concepts encourage on-site generation based on low-emission energy technologies and a high share of locally available Renewable Energy Sources (RESs) and Energy Storage Systems (ESSs). Indeed, the deployment of small to medium scales Distributed Generation (DG) based MGs (from some kilowatts to some hundreds of killoWatts) is increasingly adopted around the world. These systems can operate close to end-users with either grid-connected or islanded mode, which improves local grid reliability and resilience and increases energy efficiency[4]

Commonly a DG system can be defined as an energy source like (Photovoltaic, wind turbine…) which supplies local loads (such as remote communities, institutional and commercial applications) through a power electronic inverter and its interconnecting passive filter. For middle-power systems three-phase inverters are considered since they can handle higher power export requirements in comparison with single phase systems (used commonly in small-scale DG systems). In islanded mode the DG system is controlled in order to ensure the desired voltage characteristics at the Common Coupling Point (PCC): a voltage with a rated amplitude and frequency while maintaining a sinusoidal waveform characterized with a low rate of Total Harmonic Distortion (THD) [5,6]. The control performance is subject to numerous challenges mainly related to the load working condition which can deteriorate the power quality characterized by an increase of both voltage waveform unbalance and harmonic distortion. Indeed, the use of DG in the context of residential or commercial applications impose critical loading conditions related to the presence of nonlinear and unbalanced loads like HVAC heating and cooling systems, computer loads, lightening ballast, and most of electronic based and motor drive appliances. The voltage quality of DG systems must verify

predefined technical requirements imposed by international standards. For instance, in IEEE 1547 standard the tolerated voltage harmonic distortion at the PCC is 5%, and 3% as a maximum rate value for each individual harmonic when the load current harmonic rate is less than 20%. In IEC62040 the tolerated voltage THD is 8% while third, fifth, and seventh harmonic components must not exceed 5%, 6%, and 5% respectively[7,8].

To ensure the power quality requirements, the development of enhanced load voltage control techniques for DG systems is considered in many research works. These works include classical multi-loop control techniques [9–11], nonlinear control techniques [12–14], learning-based control methods [15–17] and predictive control techniques [18,19]. The conventional Proportional Integral (PI) controller is based on a cascade structure with two control loops i.e. an outer voltage loop and an inner current loop. This kind of control methods are cheap and simple to implement. However, under critical load conditions and due to the linearization of the system around the operating point, the performances of this control for a large scale operation are not guaranteed and can introduce saturation and reduce the overall stability margin [20]. To enhance the performance of the classical PI controller, other control techniques are proposed in literature [20–22]. In [20] a fractional PI controller has been developed motivated by its aptitude to ensure better disturbance rejection, and thereby results enhanced voltage THD. To avoid the steady-state and phase shift problems a fractional Proportional Resonant controller (PR) motivated by its aptitude to cancel the steady state error for periodic references was proposed in [5,23]. To relieve the performances of linear controllers, the use of nonlinear tracking methods is widely addressed in the literature, such as: Feedback Linearization Control (FLC) [24,25], backstepping [14,26] and Sliding Mode Control (SMC) [7,27,28]. In spite of the tracking capabilities of these controllers, some weaknesses must be overcome. For instance, FLC uses feedback variables derivatives that weaken control performance under transient modes. Furthermore, this kind of control

introduces a zero dynamics that can alter the system stability. SMC laws are commonly build up through an equivalent control based on the model and a nonlinear correction term. Despite the fact that the nonlinear correction term brings the robustness, this term induces also chattering effect that can alter the system reliability. Otherwise, with the development of high-sophisticated processors and calculators, control techniques based on learning methods such as the interactive learning control [15], the neural network control [17] and the repetitive control [16] has been adopted. However, these techniques still require too complex algorithm and they induce slow dynamic response due to the time consumed by its learning algorithm. Other studies using predictive control techniques [29,30], where commonly a deadbeat control was considered. These techniques are simple to implement, allows fast dynamic response and are flexible in front of various constraints and objectives [31,32]. However, some disadvantages remain, such as the occurrence of an undesirable resonance due to the use of a non-constant switching frequency [33,34].

In this paper, we propose to implement a robust controller based on the Interconnection and Damping Assignment Passivity Based Control (IDA-PBC) method. This technique allows guaranteeing high voltage quality in case of a standalone MG. The use of this method is motivated by its properties allowing the synthesis of control laws that guarantees the stability of the closed-loop system. In this context, IDA-PBC allows to design nonlinear controllers for systems depicted by Port Hamiltonian model. In this formalism, the Hamiltonian function is based on the energy of the system and can be viewed like Lyapunov function [35] and the control synthesis consists in shaping this energy. Consequently, the control laws ensure that the energy of the system converges to the desired equilibrium point. In view of these advantages, this method was widely devoted to the field of electrical engineering [27,36–38]. For example, it was used in [38,39] to regulate the voltage output of a three-phase inverter. The obtained results prove the performance of this technique to ensure

suitable regulation performance. As the classical IDA-PBC control techniques are based on fixed parameters, consequently, the performances of these methods decrease when the system undergoes a change in operating point.

To enhance the system robustness and manage the problem of parameter uncertainties, this paper proposes to extend the classical IDA-PBC control by adding an integral action. This technique allows reducing the effects of noises and modeling uncertainties.

The features of this paper are the following:

- Designing an IDA-PBC control that incorporates integral action to improve the stability and robustness of the system. The design of this control should follow three important steps:
  - Define the desired energy function called Hamiltonian function, this function is used to guarantee the control dynamic properties.
  - Increase the order of the system in order to build a novel desired Hamiltonian function that incorporates the integral action.
  - Synthesis of the controls laws
- Comparing robustness of the system via experimental tests to two other techniques of control: a conventional IDA-PBC and a classical PI controller.

The paper is organized as follows. The basic system description and PCH modeling are presented in section 2. A brief theoretical overview of IDA-PBC control technique is provided in section 3. Section 4, presents the controller design and the synthesis of the proposed control scheme. Section 5, introduces the other two used control, the conventional PI controller and classical IDA-PBC controller. To prove the effectiveness of the suggested controller, detailed experimental results are presented and discussed in section 6. Finally, the paper ends with a conclusion in section 7.

2. System overview and model

The studied system is illustrated in Fig. 1. It presents a typical three-phase inverter that supplies local load through an output LC filter. The DC bus is considered as an ideal voltage source with a constant value that ensures the inverter controllability. R_f, L_f and C_f represent respectively per-phase internal inductor resistance, inductance and the capacitor of the output LC filter.

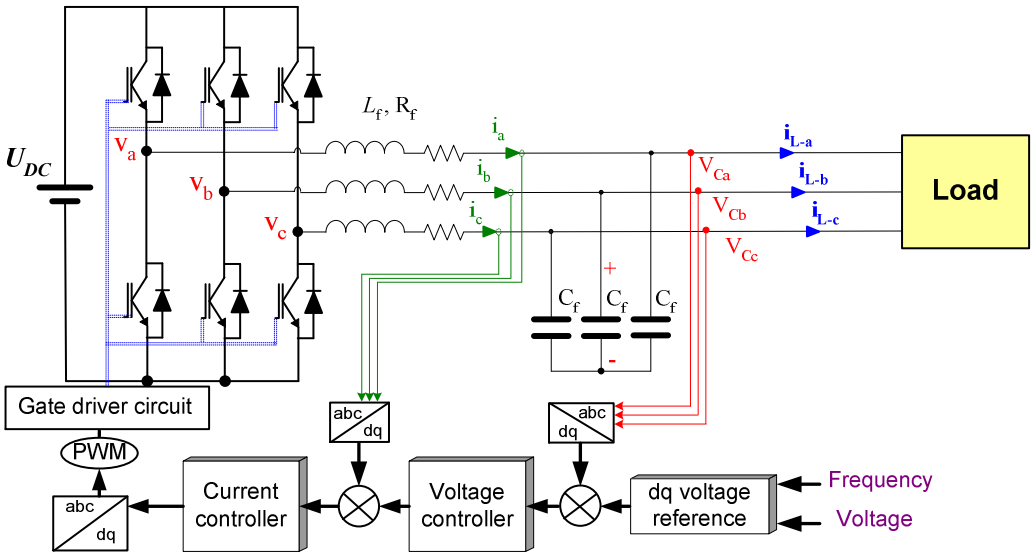

Fig. 1. Circuit scheme of the studied system.

The behavior of the studied system can be modeled by applying Kirchhoff's law. Its model is expressed by the followings equations in the rotating d-q reference.

$$\begin{aligned} L_f \frac{di_d}{dt} &= -R_f i_d + L_f \omega\, i_q + v_d - v_{Cd} \\ L_f \frac{di_q}{dt} &= -R_f i_q - L_f \omega\, i_d + v_q - v_{Cq} \\ C_f \frac{dv_{Cd}}{dt} &= i_d - i_{Ld} + C_f \omega\, v_{Cq} \\ C_f \frac{dv_{Cq}}{dt} &= i_q - i_{Lq} - C_f \omega\, v_{Cd} \end{aligned} \tag{1}$$

Where v_{Cd} ,v_{Cq} , i_d and i_q are chosen as state variables and represent respectively the dq capacitor output voltage at the PCC and the dq-component of the line currents (i_a, i_b and i_c). i_{Ld} and i_{Lq} represent the dq-components of the load currents ($i_{L\text{-}a}$, $i_{L\text{-}b}$ and $i_{L\text{-}c}$), ω is the angular frequency and v_d, v_q denote the output voltage of the inverter.

To synthesize the proposed IDA-PBC controller, the system is firstly described by Port-Control Hamiltonian (PCH) model described by the following open-loop equations [40,41] .

$$\begin{aligned} \dot{x} &= [\,\mathcal{J}(x) - \mathcal{R}(x)]\nabla H(x) + g(x)u + \xi \\ \text{y} &= g^T(\text{x})\nabla H(x) \end{aligned} \tag{2}$$

where $x \in \mathcal{R}^n$ is the state vector, $u \in \mathcal{R}^m$ is the control input vector, $y \in \mathcal{R}^m$ is the output vector with $m < n$, $g(x)$ is the input matrix that weight the action of the inputs u on the system and also on the outputs via its transpose, $H(x)$ is a smooth function of the states representing the total system energy function and $\nabla H(x)$ represents its gradient called variable of co-energy. ξ corresponds to the external perturbation vector. $\mathcal{J}(x)$ and $\mathcal{R}(x)$ are respectively the interconnection and damping matrices that verify the following form $\mathcal{R}(\text{x}) = \mathcal{R}^{\text{T}}(\text{x}) \geq 0$ and $\mathcal{J}(\text{x}) = -\mathcal{J}^{\text{T}}(\text{x})$.

In view of the studied system, the proposed Hamiltonian function expressed in (3) corresponds to the sum of the energy stored in the output LC filter.

$$H(x) = \frac{1}{2}L_f i_d^2 + \frac{1}{2}L_f i_q^2 + \frac{1}{2}C_f v_{Cd}^2 + \frac{1}{2}C_f v_{Cq}^2 \tag{3}$$

This function can be written as $H(x) = \frac{1}{2}x^T Q^{-1} x$. where $x = [x_1\ x_2\ x_3\ x_4]^T = [L_f i_d\ L_f i_q\ C_f v_{Cd}\ C_f v_{Cq}]^T$ and $Q = diag\,\{L_f \quad L_f \quad C_f \quad C_f\}$.

Afterward, the PCH form introduced in (2) can be applied to the studied system, where: $\nabla H(x) = \partial H(x)/\partial x = [i_d\ i_q\ v_{Cd}\ v_{Cq}]^T$ and the different system elements are:

$$\mathcal{R}(x) = \begin{bmatrix} R_f & 0 & 0 & 0 \\ 0 & R_f & 0 & 0 \\ 0 & 0 & 0 & 0 \\ 0 & 0 & 0 & 0 \end{bmatrix} \tag{4.a}$$

$$g(x) = \begin{bmatrix} 1 & 0 \\ 0 & 1 \\ 0 & 0 \\ 0 & 0 \end{bmatrix} \tag{4.b}$$

$$u = \begin{bmatrix} v_d \\ v_q \end{bmatrix} \tag{4.c}$$

$$\mathcal{J}(x) = \begin{bmatrix} 0 & L_f\omega & -1 & 0 \\ -L_f\omega & 0 & 0 & -1 \\ 1 & 0 & 0 & C_f\omega \\ 0 & 1 & -C_f\omega & 0 \end{bmatrix} \tag{4.d}$$

$$\xi = \begin{bmatrix} 0 \\ 0 \\ -i_{Ld} \\ -i_{Lq} \end{bmatrix} \tag{4.e}$$

3. Background of control strategy on IDA PBC

The PBC is a kind of control that stabilizes the system by making it dissipative, in other word make it passive. This control technique consists to identify the natural energy function of the system called $H(x)$ and then to find a static state-feedback control $u = \beta(x)$ that ensure a closed-loop dynamics system conform also to the PCH form.

$$\dot{x} = [\, \mathcal{J}_\mathrm{d}(x) - \mathcal{R}_\mathrm{d}(x)]\nabla H_\mathrm{d}(x) \tag{5}$$

In this expression the desired energy function $H_d(x)$ is characterized by a local minimum at the desired equilibrium point x^*. The desired interconnection and damping matrices fulfill respectively the following conditions: $\mathcal{J}_\mathrm{d}(x) = -\mathcal{J}_\mathrm{d}^\mathrm{T}(x)$ and $\mathcal{R}_\mathrm{d}(\mathrm{x}) = \mathcal{R}_\mathrm{d}^\mathrm{T}(x) \geq 0$.

In order to calculate the control input u, the designer must solve the matching equation between the former closed-loop equation (5) and that of open-loop defined by (2). This matching system is defined by:

$$[\mathcal{J}(x) - \mathcal{R}(x)]\nabla H(x) + g(x)\beta(x) + \xi = [\mathcal{J}_{\mathrm{d}}(x) - \mathcal{R}_{\mathrm{d}}(x)]\nabla H_{\mathrm{d}}(x) \quad (6)$$

3.1. Conventional IDA-PBC approach

In order to solve the matching equation (6), the state-feedback control $u = \beta(x)$ may be obtained by using new matrices $\mathcal{J}_a(x)$, $\mathcal{R}_a(x)$ and a vector function, designated by $K(x)$. These components are defined by the control designer to underline some characteristics and to ensure simplifications.

$$[(\boldsymbol{\mathcal{J}}(\boldsymbol{x}) + \boldsymbol{\mathcal{J}_a}(\mathbf{x})) - (\boldsymbol{\mathcal{R}}(\boldsymbol{x}) + \boldsymbol{\mathcal{R}_a}(\boldsymbol{x}))]\boldsymbol{K}(\boldsymbol{x}) = -[\boldsymbol{\mathcal{J}_{\mathrm{a}}}(\boldsymbol{x}) - \boldsymbol{\mathcal{R}_{\mathrm{a}}}(\boldsymbol{x})]\boldsymbol{\nabla H}(\boldsymbol{x}) + \boldsymbol{g}(\boldsymbol{x})\boldsymbol{\beta}(\boldsymbol{x}) + \boldsymbol{\xi} \quad (7)$$

The added expressions must verify the next properties [42]:

(i) Structure preservation: $\mathcal{R}_d(x) = \mathcal{R}(x) + \mathcal{R}_a(x) = \mathcal{R}_{\mathrm{d}}^{\mathrm{T}}(\mathrm{x}) \geq 0$ and $\mathcal{J}_d(x) = \mathcal{J}(x) + \mathcal{J}_a(x) = -\mathcal{J}_{\mathrm{d}}^{\mathrm{T}}(x)$.

(ii) Integrability: $K(x)$ is the gradient of a scalar function: $\nabla K(x) = [\nabla K(x)]^T$.

(iii) Equilibrium assignment: $K(x)$ at x^* satisfies: $K(x^*) = -\nabla H(x^*)$

(iv) Lyapunov stability: the Jacobian of $K(x)$ at x^* satisfies the bound: $\nabla K(x^*) > -\nabla^2 H(x^*)$.

A fifth condition must also be verified if the invariance of the equilibrium point is not assured according to the Lyapunov theorem. In this case, some researchers impose to use the LaSalle theorem to ensure the invariance of the equilibrium point [43].

$$-[\nabla H_d]^T \mathcal{R}_d(x)\nabla H_d 0 \leq 0 \quad (8)$$

This additional condition ensures that the chosen desired function H_d allows getting a bounded solution.

By checking all these conditions the closed loop system $u = \beta(x)$ will be a Port-Controlled with: $K(x) = \nabla H_a(x)$ where $H_d(x) = H(x) + H_a(x)$.

Depending on control's objective and on desired proprieties, the designer of the control laws is free to select the elements constituting the matrices $\mathcal{R}_a(x)$ and $\mathcal{J}_a(x)$. For instance, in case of electrical power systems, the matrix of interconnection is usually taken in order to compensate the coupling between *dq*-axis, in the other hand, the damping matrix is chosen to improve the convergence dynamic.

3.2. Robust IDA-PBC with integral action

In order to enhance the dynamic and the control performances under model uncertainties, an integral action can be added while conserving the Hamiltonian form [35,40,44]. The addition of this action allows also to cancel steady-state error and to increase the robustness of systems under parameters uncertainties and other constant disturbances.

The synthesis of the control need two steps. The first one is the same as in the classical IDA-PBC and the second one consists in extending the closed-loop system by adding an integral action as described below. The augmented system is described by:

$$\begin{bmatrix} \dot{x} \\ \dot{x}_e \end{bmatrix} = \begin{bmatrix} J_d(x) - R_d(x) & g(x)K_I \\ -K_I\, g^T(x) & 0 \end{bmatrix} \begin{bmatrix} \nabla_x H_{de} \\ \nabla_{x_e} H_{de} \end{bmatrix} \tag{9}$$

where x_e is the state vector that reflects the additional integral action, K_I is the matrix of integral gain that verifies $K_I = K_I^T \geq 0$ and H_{de} will be the new desired Hamiltonian function. This one verify that $H_{de}(x, x_e) = H_d(x, x_e) + (x_e^T K_I^{-1} x_e)/2$.

The state variables in case of PCH form can be separated in two groups [41]:

- Relative-Degree-One (RD1) states: this group of state variables characterizes state variables which are directly related to the input u.

- Higher-Relative-Degree (HRD) states: it groups the state-variables indirectly related to the system input. So the relation with the input control can be created after derivation.

The additional integral action can be added to any kind of state variable (RD1 or HRD) [41]. In this studied system, the mean objective is to regulate the voltage at the inverter output. As a suitable choice to this objective, the integral action will be associated to the HRD state described in the dq-framework.

The change of state is ensured by considering z_1, z_h and z_e respectively the RD1 states, the HRD states and the extended integral term. After the change of state, the expanded form of the IDA-PBC because of adding the integral term to the HRD states can be expressed as:

$$\begin{bmatrix} \dot{z_1} \\ \dot{z_h} \\ \dot{z_e} \end{bmatrix} = \begin{bmatrix} J_1^d - R_1^d & J_{1h}^d - R_{1h}^d & 0 \\ J_{h1}^d - R_{h1}^d & J_h^d - R_h^d & -K_I \\ 0 & K_I^T & 0 \end{bmatrix} \begin{bmatrix} \nabla_{z_1} H_{dz} \\ \nabla_{z_h} H_{dz} \\ \nabla_{x_e} H_{dz} \end{bmatrix} = [\mathcal{J}_{\mathrm{d}}(\mathrm{z}) - \mathcal{R}_{\mathrm{d}}(\mathrm{z})] \nabla H_{dz} \tag{10}$$

This expression highlights a new desired energy or Hamiltonian function computed at the new states variables z_1, z_h, and the quadratic term z_e. The desired Hamiltonian function have the following expression.

$$H_{dz}(z_1, z_h, z_e) = H_d(z_1, z_h) + \frac{z_e^T K_I^{-1} z_e}{2} \tag{11}$$

The change of state has been ensured by the following expression:

$z_e = x_e$

$z_h = x_h$

and $z_1 = \psi(x_1, x_h, x_e)$,

where, in order to calculate z_1, the designer must verify (12).

$$\begin{aligned} &(J_{h1}^d(z) - R_{h1}^d(z)) \nabla_{z_1} H_{dz} + (J_h^d(z) - R_h^d(z)) \nabla_{z_h} H_{dz} - K_I \nabla_{z_e} H_{dz} \\ &= (J_{h1}^d(x) - R_{h1}^d(x)) \nabla_{x_1} H_d + (J_h^d(x) - R_h^d(x)) \nabla_{x_h} H_d \end{aligned} \tag{12}$$

4. Realization of the IDA-PBC with integral action

This section details the realization of the proposed IDA-PBC-IA. The control synthesis consists of three steps. The first one is to propose an initial desired function, which is the Hamiltonian function. The second step is to add the expected integral action by extending the order of the system, and finally, calculate the control law using the matching equations described in (6).

The overall view of the control to design is presented in Fig. 2.

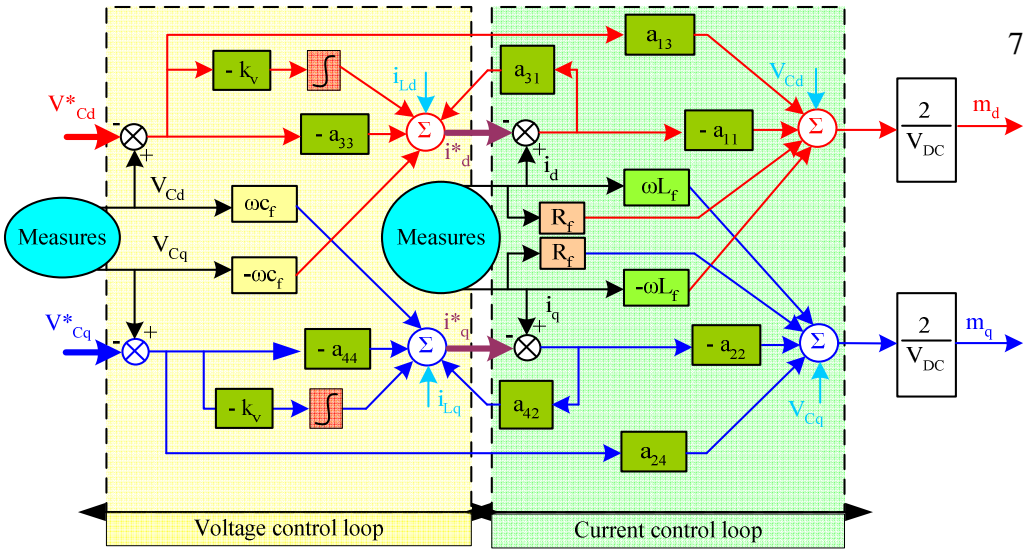

Fig. 2. Block diagram of the proposed control approach.

The desired Hamiltonian function depend on the control objective. It has a local minimum at the desired equilibrium point x^*. By considering the open-loop function defined by (2), the desired function is given by.

$$\begin{aligned} H_d(x) &= \frac{1}{2}L_f(i_d - i_d^*)^2 + \frac{1}{2}L_f\left(i_q - i_q^*\right)^2 + \frac{1}{2}C_f(v_{Cd} - {v_{Cd}}^*)^2 + \frac{1}{2}C_f\left(v_{Cq} - {v_{Cq}}^*\right)^2 \\ &= \frac{1}{2L_f}(x_1 - {x_1}^*)^2 + \frac{1}{2L_f}(x_2 - {x_2}^*)^2 + \frac{1}{2C_f}(x_3 - {x_3}^*)^2 + \frac{1}{2C_f}(x_4 - {x_4}^*)^2 \end{aligned} \tag{13}$$

Formally, to conserve the original form of the interconnection and damping matrices ($\mathcal{J}(\mathrm{x})$ and $\mathcal{R}(\mathrm{x})$), the candidate desired matrices can be expressed as:

$$[\,\mathcal{J}_\mathrm{d}(x) - \mathcal{R}_\mathrm{d}(x)] = \begin{bmatrix} -a_{11} & 0 & a_{13} & 0 \\ 0 & -a_{22} & 0 & a_{24} \\ a_{31} & 0 & -a_{33} & 0 \\ 0 & a_{42} & 0 & -a_{44} \end{bmatrix} \tag{14}$$

where : $\mathrm{a}_{13} = -\mathrm{a}_{31}$, $\mathrm{a}_{24} = -\mathrm{a}_{42}$ and $\mathrm{a}_{\mathrm{ii}} \geq 0$ with $i = \{1, 2, 3, 4\}$.

Once fixed the desired function, the second step is to incorporate the integral action as presented in equation (10) and then express the system in the new state variable (z). For this representation, the following assumptions are made:

- The states z_1 and z_h which are relied respectively to RD1 and HRD as it is presented in (9) regroup the dq-line currents and the dq-capacitor voltages noted by $(z_{1d}, z_{1q})$and (z_{hd}, z_{hq}).
- The new added state variables z_5 and z_6 are chosen as follow:

$$z_5 = \int (v_{Cd} - v_{Cd}^*); z_6 = \int (v_{Cq} - v_{Cq}^*).$$

Therefore, taking into account all these assumptions, the new candidate desired interconnection and damping matrices will have the following form:

$$[\mathcal{J}_{\mathrm{d}}(\mathrm{z}) - \mathcal{R}_{\mathrm{d}}(\mathrm{z})] = \begin{bmatrix} -\mathrm{a}_{11} & 0 & \mathrm{a}_{13} & 0 & 0 & 0 \\ 0 & -\mathrm{a}_{22} & 0 & \mathrm{a}_{24} & 0 & 0 \\ \mathrm{a}_{31} & 0 & -\mathrm{a}_{33} & 0 & -k_V & 0 \\ 0 & \mathrm{a}_{42} & 0 & -\mathrm{a}_{44} & 0 & -k_V \\ 0 & 0 & k_V & 0 & 0 & 0 \\ 0 & 0 & 0 & k_V & 0 & 0 \end{bmatrix} \tag{15}$$

where k_v is the gain which represents the integral terms.

Noted that by considering that the integral effect presented in state variable z_{1d} and z_{1q} is equal to zero and applying the matching equation (12), the chosen new state variable z preserves the matrix (14) and the Hamiltonian form.

As a consequence, the new desired Hamiltonian expressed in z state variable in (16) is in the form of which it was expressed in the "x" state variable in (11).

$$\begin{aligned} H_{dz}(z) = {} & \frac{1}{2L_f}(z_1 - {z_1}^*)^2 + \frac{1}{2L_f}(z_2 - {z_2}^*)^2 + \frac{1}{2C_f}(z_3 - {z_3}^*)^2 + \frac{1}{2C_f}(z_4 - {z_4}^*)^2 \\ & + \frac{1}{2}k(z_5 - {z_5}^*)^2 + \frac{1}{2}k(z_6 - {z_6}^*)^2 \\ = {} & H_d(x) + (z_e^T K_I^{-1} z_e)/2 \end{aligned} \tag{16}$$

Fig. 3 illustrates the evolution of the energy $H_{dz}(z)$ according to the state variables z_3 and z_4 where, for two chosen values for the gain k_I ($k_I = 10$; $k_I = 5$), the current loop is assumed perfect with $z_1 = z_1{}^*$ and $z_2 = z_2{}^*$. It is shown that by increasing the gain the convergence towards the equilibrium point x^* is enhanced.

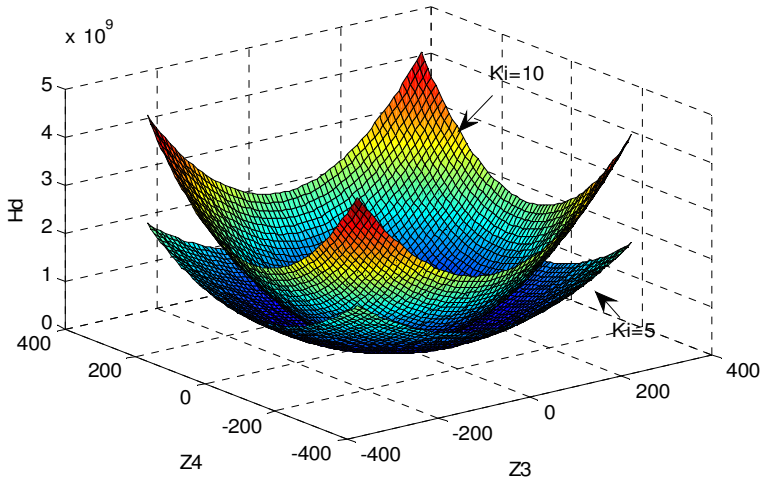

Fig. 3. Evolution of the energy $H_{dz}(z)$ according to state variable.

The last task of control design is to calculate the control laws. These latter are obtained by solving the matching equations expressed in (6) between the closed-loop and that of open-loop defined previously in (2).

To conclude, two nested control loops are to be defined. The outer one generates the line currents reference in the dq- framework and it is described by:

$$\begin{aligned} i_d^* &= a_{31}(i_d - i_d^*) - a_{33}(v_{Cd} - v_{Cd}^*) - k_V \int (v_{Cd} - v_{Cd}^*)\, dt + i_{Ld} - C_f \omega v_{Cq} \\ i_q^* &= a_{42}(i_q - i_q^*) - a_{44}(v_{Cq} - v_{Cq}^*) - k_V \int (v_{Cq} - v_{Cq}^*)\, dt + i_{Lq} + C_f \omega v_{Cd} \end{aligned} \tag{17}$$

And the inner one generates the input reference of voltages to the inverter has the following expressions:

$$\begin{aligned} v_d^* &= -a_{11}\,(i_d - i_d^*) + a_{13}(v_{Cd} - v_{Cd}^*) + R_f i_d - L_f \omega i_q + v_{Cd} \\ v_q^* &= -a_{22}\,(i_q - i_q^*) + a_{24}(v_{Cq} - v_{Cq}^*) + R_f i_q + L_f \omega\, i_d - v_{Cq} \end{aligned} \tag{18}$$

Stability verification

This part presents the verification of the conditions necessary to ensure that the system is locally stable at the point of equilibrium x^* by applying the proposed controller based on the passivity. The conditions already studied in section (3.1) are checked.

i. Structure preservation:

$$\mathcal{J}_d(z) = \begin{bmatrix} 0 & 0 & a_{13} & 0 & 0 & 0 \\ 0 & 0 & 0 & a_{24} & 0 & 0 \\ a_{31} & 0 & 0 & 0 & -k_I & 0 \\ 0 & a_{42} & 0 & 0 & 0 & -k_I \\ 0 & 0 & k_I & 0 & 0 & 0 \\ 0 & 0 & 0 & k_I & 0 & 0 \end{bmatrix} = -[\mathcal{J}_d(z)]^T \tag{19.a}$$

$$\mathcal{R}_d(z) = \begin{bmatrix} \mathrm{a}_{11} & 0 & 0 & 0 & 0 & 0 \\ 0 & \mathrm{a}_{22} & 0 & 0 & 0 & 0 \\ 0 & 0 & \mathrm{a}_{33} & 0 & 0 & 0 \\ 0 & 0 & 0 & \mathrm{a}_{44} & 0 & 0 \\ 0 & 0 & 0 & 0 & 0 & 0 \\ 0 & 0 & 0 & 0 & 0 & 0 \end{bmatrix} = [\mathcal{R}_d(z)]^T > 0 \tag{19.b}$$

where $\mathrm{a}_{13} = -\mathrm{a}_{31}$, $\mathrm{a}_{24} = -\mathrm{a}_{42}$; $\mathrm{a}_{\mathrm{ii}} \geq 0$ et $k_I > 0$, where $i = \{1, 2, 3, 4\}$.

➔ The first structural condition (i) is well verified

ii. Integrability:

$$\begin{aligned} H_a(z) &= H_{dz}(z) - H(z) \\ &= \left[\frac{1}{2L_f}(z_1 - {z_1}^*)^2 + \frac{1}{2L_f}(z_2 - {z_2}^*)^2 + \frac{1}{2C_f}(z_3 - {z_3}^*)^2 + \frac{1}{2C_f}(z_4 - {z_4}^*)^2 \right. \\ &\qquad \left. + \frac{1}{2}k_I(z_5 - {z_5}^*)^2 + \frac{1}{2}k_I(z_6 - {z_6}^*)^2\right] - \left[\frac{1}{2}\frac{{z_1}^2}{L_f} + \frac{1}{2}\frac{{z_2}^2}{L_f} + \frac{1}{2}\frac{{z_3}^2}{C_f} + \frac{1}{2}\frac{{z_4}^2}{C_f}\right] \\ &= \frac{1}{2L_f}\left({z_1}^{*2} + {z_2}^{*2}\right) - \frac{1}{L_f}(z_1{z_1}^* + z_2{z_2}^*) + \frac{1}{2C_f}\left({z_3}^{*2} + {z_4}^{*2}\right) \\ &\qquad - \frac{1}{C_f}(z_3{z_3}^* + z_4{z_4}^*) + \frac{1}{2}k_I(z_5 - {z_5}^*)^2 + \frac{1}{2}k_I(z_6 - {z_6}^*)^2 \end{aligned} \tag{20}$$

$$K(z) = \frac{\partial H_a(z)}{\partial z} = \left[-\frac{1}{L_f}{z_1}^*, -\frac{1}{L_f}{z_2}^*, -\frac{1}{C_f}{z_3}^*, -\frac{1}{C_f}{z_4}^*, k_I(z_5 - z_5^*), k_I(z_6 - z_6^*)\right]^T \tag{21}$$

where $K(z) = [K_1, K_2, K_3, K_4, K_5, K_6]^T$

$$\frac{\partial K_1(z)}{\partial z_i} = 0; \frac{\partial K_2(z)}{\partial z_i} = 0; \frac{\partial K_3(z)}{\partial z_i} = 0; \frac{\partial K_4(z)}{\partial z_i} = 0; \frac{\partial K_5(z)}{\partial z_i} = k_I; \frac{\partial K_6(z)}{\partial z_i} = k_I \tag{22}$$

where $i = \{1, 2, 3, 4,5,6\}$.

This proves that the second condition of integrability (ii) is verified.

iii. Equilibrium assignment:

Using the equation (21)

And considering the equilibrium point: $z^* = ({z_1}^*, {z_2}^*, {z_3}^*, {z_4}^*, {z_5}^*, {z_6}^*)$.

it gives

$$K(z^*) = \frac{\partial H_a(z^*)}{\partial z} = \left[-\frac{1}{L_f}{z_1}^*, -\frac{1}{L_f}{z_2}^*, -\frac{1}{C_f}{z_3}^*, -\frac{1}{C_f}{z_4}^*, 0,0\right] \quad (23)$$

On the other hand

$$-\nabla H(z^*) = \left[-\frac{1}{L_f}{z_1}^*, -\frac{1}{L_f}{z_2}^*, -\frac{1}{C_f}{z_3}^*, -\frac{1}{C_f}{z_4}^*, 0,0\right] \quad (24)$$

➔This proves that the equilibrium condition (iii) is well verified.

iv. Lyapunov stability:

$$-\nabla_z^2 H_{dz}(z^*) = \frac{\partial^2 H_{dz}(z^*)}{\partial z^2} = \frac{2}{L_f} + \frac{2}{C_f} + 2k_I > 0 \quad (25)$$

where L_f, C_f and k_I are positive coefficients. This fourth condition (iv) is checked.

Moving to the fifth condition to verify the invariance of the equilibrium point by Lasalle's theorem.

$$-[\nabla H_{dz}]^T \mathcal{R}_d(z) \nabla H_{dz} = \begin{bmatrix} -\frac{10}{L_f}(z_1 - {z_1}^*)^2 \\ -\frac{10}{L_f}(z_2 - {z_2}^*)^2 \\ -\frac{10}{C_f}(z_3 - {z_3}^*)^2 \\ -\frac{10}{C_f}(z_4 - {z_4}^*)^2 \\ 0 \\ 0 \end{bmatrix} \leq 0 \quad (26)$$

This further proves that the equilibrium point is an invariant point and the chosen H_{dz} ensures that the solution is bounded.

This subset verifies that the applied control ensures local stability of the equilibrium point of the closed-loop system.

5. Comparative controllers

To evaluate the performance of the proposed controller, a comparison test with the classical PI controller and the conventional IDA-PBC in the experimental part (section 6) will be provided. In the following, a brief description of each type of control technique is given.

5.1. Classical PI controller

Fig. 4 presents the scheme of the used classical PI controller based on cascaded loops. It is composed of an outer voltage loop and an inner current loop. The regulation of the output voltage of the capacitor filter C_f allows generating the reference output inverter current measured through the inductor L_f.

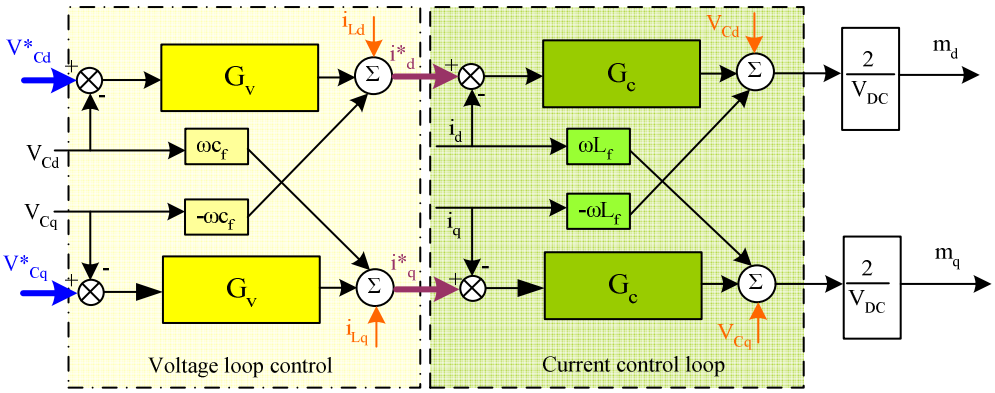

Fig. 4. Block diagram of the PI controller using nested loops.

The control laws are described by the following expressions:

$$\begin{aligned} i_d^* &= G_V(s)(v_{Cd} - v_{Cd}^*) + i_{Ld} - C_f\omega v_{Cq} \\ i_q^* &= G_V(s)\left(v_{Cq} - v_{Cq}^*\right) + i_{Lq} + C_f\omega v_{Cd} \\ v_d^* &= G_C(s)(i_d^* - i_d) + R_f i_d - L_f\omega\, i_q + v_{Cd} \\ v_q^* &= G_C(s)\left(i_q^* - i_q\right) + R_f i_q + L_f\omega\, i_d + v_{Cq} \end{aligned} \tag{27}$$

where $G_V(s) = k_{pV} + \frac{k_{iV}}{s}$ and $G_C(s) = k_{pC} + \frac{k_{iC}}{s}$ present respectively the PI transfer functions of the outer and inner loops.

The closed-loop transfer functions for the two control loops are:

$$H_C(s) = \frac{\left(\frac{k_{pC}}{L_f}\right)s + \left(\frac{k_{iC}}{L_f}\right)}{s^2 + \left(\frac{k_{pC}}{L_f}\right)s + \left(\frac{k_{iC}}{L_f}\right)}$$
$$H_V(s) = \frac{\left(\frac{k_{pV}}{C_f}\right)s + \left(\frac{k_{iV}}{C_f}\right)}{s^2 + \left(\frac{k_{pV}}{C_f}\right)s + \left(\frac{k_{iV}}{C_f}\right)} \quad (28)$$

These two functions have the form of a second-order system, and by applying the pole placement technique for this type of system, the controller parameters of each of these two loops can be deduced respectively ($k_{pC} = 2\,\xi_C L_f \omega_C$, $k_{iC} = L_f\,\omega_C^2$) and ($k_{pV} = 2\,\xi_V C_f \omega_V$, $k_{iV} = C_f\,\omega_V^2$), where ξ_C and ω_C are respectively the desired damping factor and bandwidth of the current loop, and ξ_V and ω_{CV} are the desired damping factor and bandwidth of the voltage loop.

The external loop is designed to enhance the performance of the system in the steady-state and get the desired voltage at the output. On the other hand, the inner loop acting on the dynamic performance to ensure good disturbance rejection. The bandwidth of the outer loop of voltage (fixed by ω_v) is designed to be ten-time less than the inner loop of current (fixed by ω_C). For that in this control test, the damping factors ξ_C and ξ_V are set to 0.7. The current loop bandwidth is fixed to 2000 rad/s, while the voltage one is set to 200 rad/s.

5.2. Conventional IDA-PBC controller

As presented in section (3.1), the design of a conventional IDA-PBC control is derived through the resolution of the matching equation (6). The control to be applied is composed of two nested loops and is presented in the following Fig. 5. The outer loop calculates the reference inner loop currents.

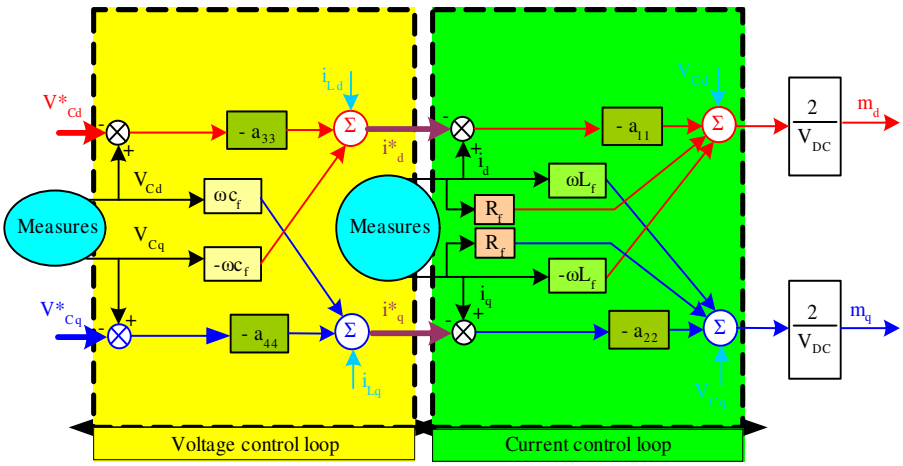

Fig. 5. Block diagram of the used classical IDA-PBC controller.

$$\begin{aligned} i_d^* &= -a_{33}(v_{Cd} - v_{Cd}^*) + i_{Ld} - C_f \omega v_{Cq} \\ i_q^* &= -a_{44}(v_{Cq} - v_{Cq}^*) + i_{Lq} + C_f \omega v_{Cd} \end{aligned} \tag{29}$$

The inner loop provides the output voltage reference.

$$\begin{aligned} v_d^* &= -a_{11}\,(i_d - i_d^*) + R_f i_d - L_f \omega i_q + v_{Cd} \\ v_q^* &= -a_{22}\,(i_q - i_q^*) + R_f i_q + L_f \omega\, i_d + v_{Cq} \end{aligned} \tag{30}$$

6. Comparative experimental results

To validate the proposed approach of control, detailed experimental tests are performed using a dSPACE 1007 rapid prototyping system. The proposed controller performances are compared to those of a classical PI controller and a conventional IDA PBC control presented in section 5. The power circuit and control parameters are listed in TABLE I. Fig. 6. shows the experimental test bench.

The execution times of the three compared controllers are measured to highlight the effectiveness of each controller according to the computational time. The corresponding execution time is about: 30.4µs with the PI controller, 26.5µs for the classical IDA-PBC controller and 30.9 µs using the proposed IDA-PBC-IA controller.

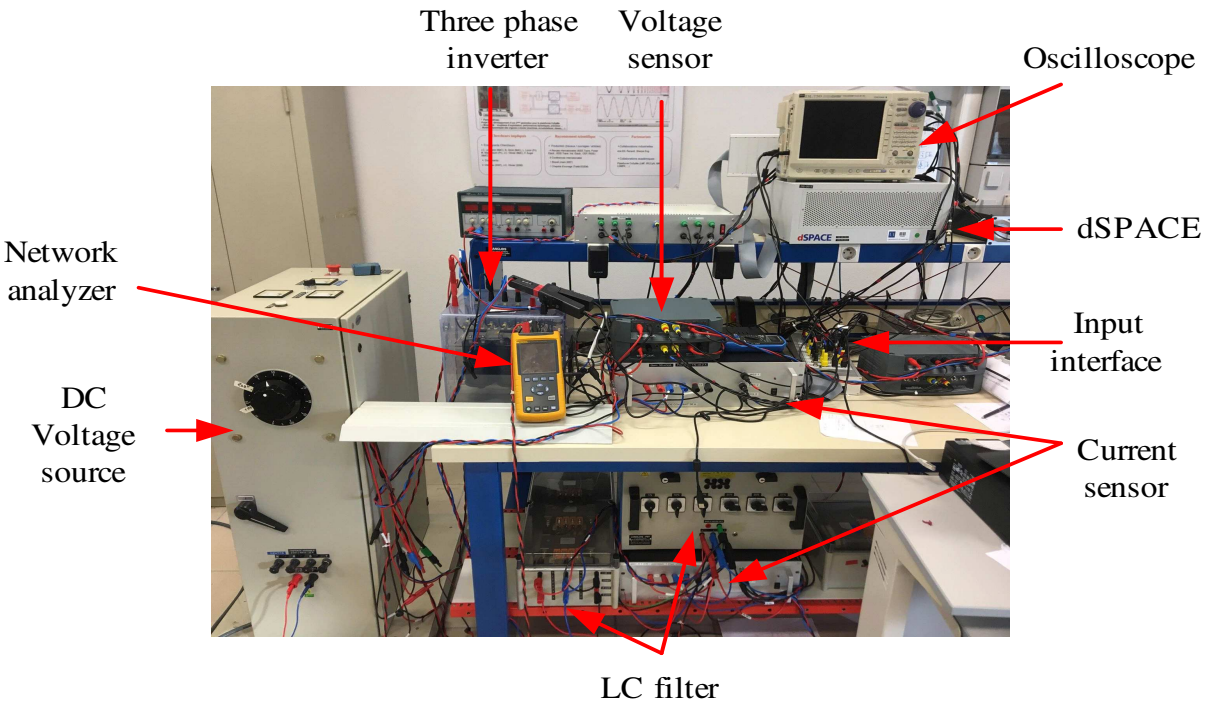

Fig. 6. Experimental test bench of the studied system.

TABLE I. System and control parameters.

System Parameters	**Control Parameters**		
	PI Controller	**Conventional IDA-PBC**	**IDA-PBC-IA**
$L_f = 3mH$	k_{iV}=2.82	$a_{11} = a_{22}$ =10	$a_{11} = a_{22} = 10$
$R_f = 0.1\ \Omega$	k_{pV}=0.024	$a_{33} = a_{44} = 1$	$a_{33} = a_{44} = 1$
$C_f = 44\mu F$	k_{iC}=16922	$a_{13} = -a_{31}$=1	$a_{13} = -a_{31}$=1
$U_{DC} = 450V$	k_{pC}=14.15	$a_{24} = -a_{42}$=1	$a_{24} = -a_{42}$=1
$F_s = 10kHz$			k_V=10

The used voltage and current sensor specification are listed in the following TABLE II.

TABLE II. Used sensors specification

Sensor equipment	**Specification**
Voltage sensor	Differential probe MTX 1032-C
Current sensor	A current measuring box characterized by 50mV/A; Current max 36A; Precision 1% ± 0.2A; Offset 300mA

6.1. Dynamic test under linear load

6.1.1. Step of Load

In this test, a step load from 0 to 2kW is performed, the resulted RMS voltage and its corresponding three-phase voltages and load currents obtained with the three compared controllers are presented respectively in Fig. 7. Herein, the RMS voltage is calculated by

$$V_{RMS} = \sqrt{\frac{1}{3}\left(v_{Ca}{}^2 + v_{Cb}{}^2 + v_{Cc}{}^2\right)} \tag{31}$$

It can be seen that the proposed controller allows better rejection of disturbance than the other controllers at the instant of the step load.

The voltage drop is about 12V with the proposed method while it exceeds 30V with the conventional IDA-PBC and a classical PI. In the same time, the recovery time is about 3,26ms with the proposed control, while it's about 5,28ms and 6,38ms with the comparative controllers, respectively classical IDA-PBC and PI controller.

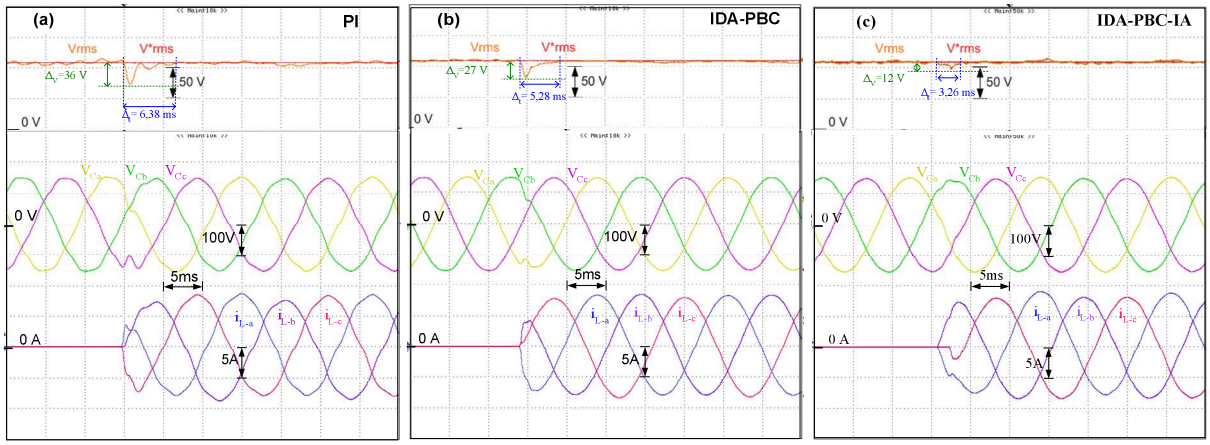

Fig. 7. Comparative experimental results showing the RMS voltage, the three-phase voltage and the load currents in case of a step load from zero to 2kW (a) classical PI controller, (b) conventional IDA-PBC, (c) proposed IDA-PBC-IA controller.

In terms of voltage quality, the obtained THD values with the compared controllers are summarized in TABLE III.

TABLE III. THD variation for linear load

Control	*PI*	*IDA-PBC*	*IDA-PBC-IA*
THDv (%)	1%	0,8%	0,7%

6.1.2. Start-up

The following experimental results evaluate the system start-up performances with the three compared controllers. The output voltage RMS is changed from 0 V to 110 V.

Fig. 8 (a, b and c) show respectively the RMS voltage, the three phase voltage and the load currents obtained respectively with a classical PI controller, conventional IDA-PBC and the proposed control strategy. As it can be appreciated in Fig. 8, the proposed control ensures the faster start-up response than the conventional IDA-PBC and the classical PI.

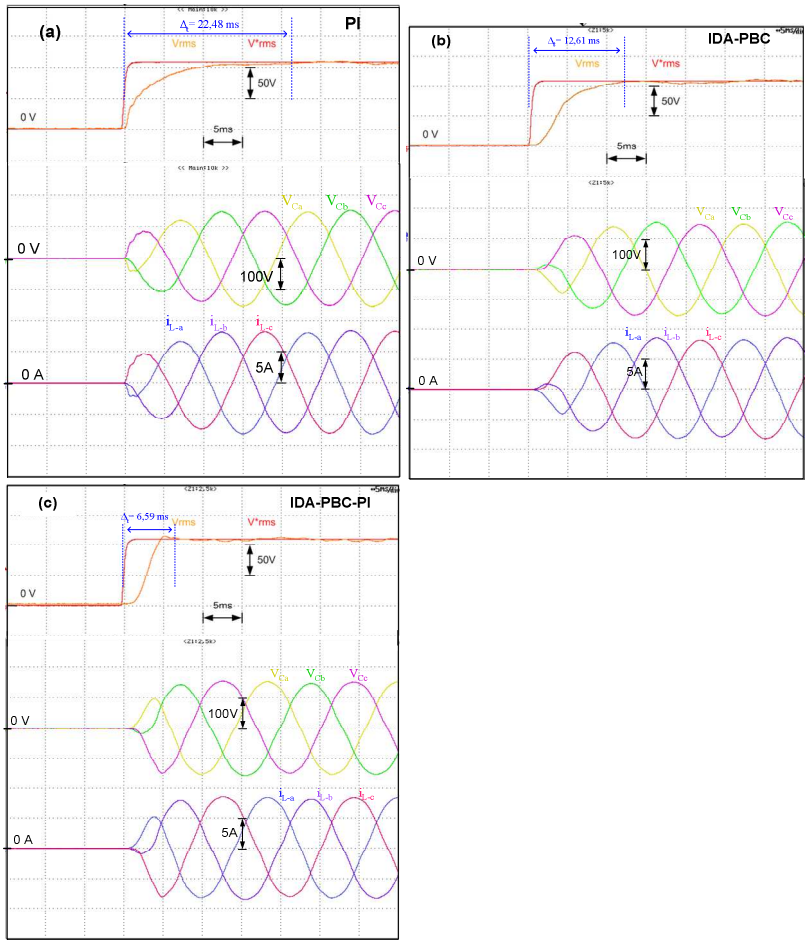

Fig. 8. Comparative experimental results showing the RMS voltage, the three-phase voltage and load currents in case of start-up reference voltage from 0 to 110 V (a) classical PI controller, (b) conventional IDA-PBC, (c) proposed IDA-PBC-IA controller.

6.1.3. Unbalanced load conditions

Fig. 9 illustrates the effectiveness of the three compared controllers under unbalanced load condition. For this aim, the phase load 'a' is disconnected as it can be appreciated in Fig. 9. The obtained THD values are reported in TABLE IV. From these results, it can be seen that the proposed control shows a better performance under unbalance load condition than those of the conventional IDA-PBC and the classical PI.

TABLE IV. THD variation for unbalanced load conditions.

Control	***PI***	***IDA-PBC***	***IDA-PBC-IA***
THDv (%)	4,55%	2,62%	2,38%

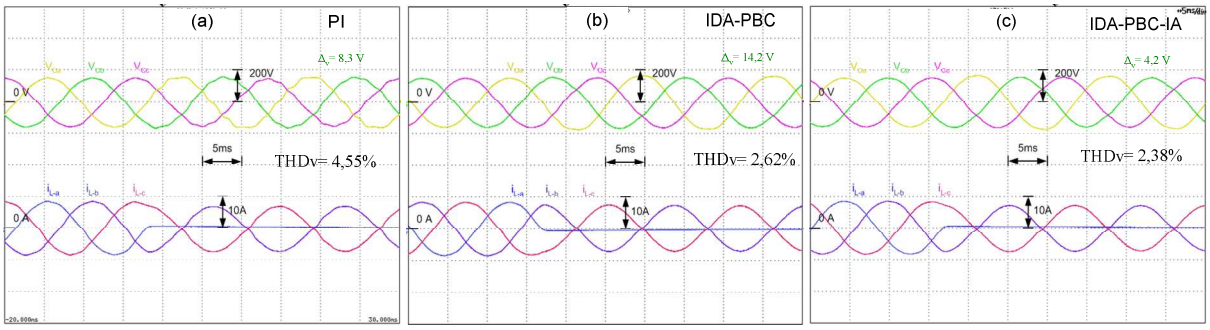

Fig. 9. Comparative experimental results in case of unbalanced load with phase 'a' suddenly opened: (a) classical PI controller, (b) conventional IDA-PBC, (c) proposed IDA-PBC-IA controller.

6.2. Parametric robustness test

In order to evaluate the robustness of the three compared control techniques, the physical values of the output LC filter are changed. The following TABLE V and TABLE VI report the result of the resulted THD rates obtained with the compared controllers. The presented results highlight that the proposed control techniques are maintained in the case of large filter parameters variation.

TABLE V. Line inductor variation

L_f		**-50%**	**Nominal**	**+50%**
THDv (%)	***IDA-PBC***	1.25%	0.8%	1.3%
	Proposed IDA-PBC-IA	1%	0.7%	1.1%

	PI	1.4%	1%	1.6%

TABLE VI. Capacitor filter variation

Cf		***-50%***	***Nominal***	***+50%***
THDv (%)	***IDA-PBC***	1%	0.8%	1%
	Proposed IDA-PBC-IA	0.9%	0.7%	0.9%
	PI	1.7%	1%	1.2%

6.3. Nonlinear load conditions

In this part, the three compared controllers are evaluated under a nonlinear load (three phase diode bridge rectifiers) as shown in Fig. 10. The output capacitor value is 100µF and the resistor is set to 35Ω. Fig. 11 illustrates the resulted harmonic components of the load current where its corresponding THD rate is 58,27%.

Fig. 12 shows the behavior of the output voltage and the form of the load currents obtained with the three compared controllers respectively: classical PI, conventional IDA-PBC, and the proposed IDA-PBC-IA. The harmonic spectrums of the obtained output voltage are presented in Fig. 13. The obtained THD rates by the three compared controllers are conform to IEEE 1547-2014 standard. Furthermore, this figure highlights the superiority of the proposed controller that shows 3.1% as a THD. This THD rate value is about 3.5% and 4.2% with respectively the conventional IDA-PBC and the classical PI.

Fig. 10. Diodes bridge rectifier used as a nonlinear load.

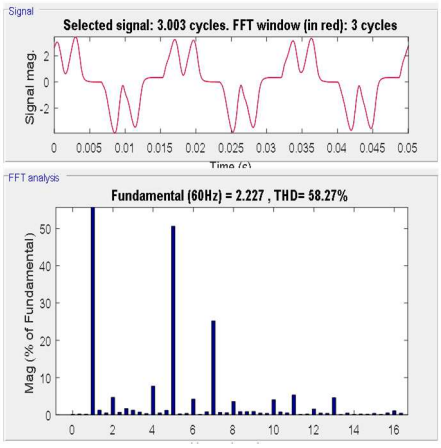

Fig. 11. Supplied load current waveforms and its corresponding harmonic components.

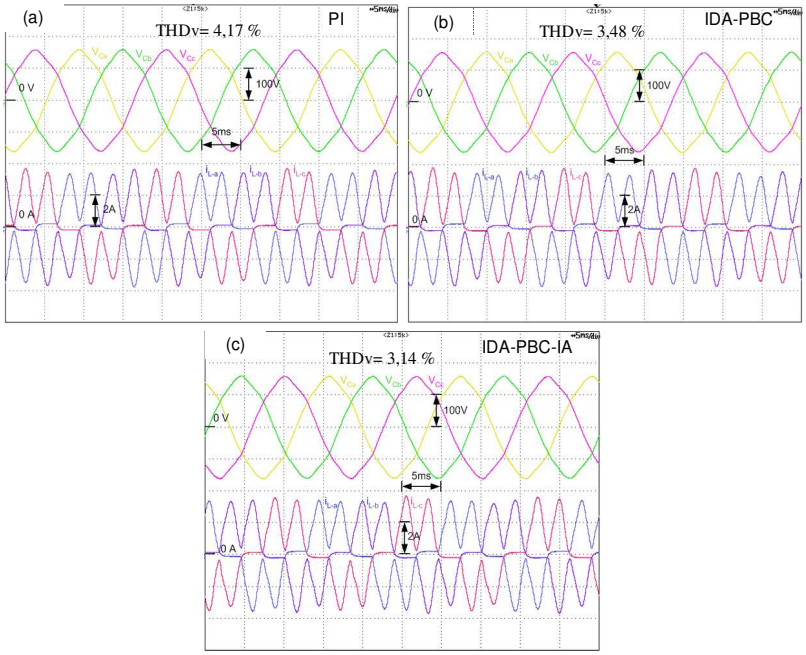

Fig. 12. Output voltage and current waveforms in response to nonlinear load conditions: (a) classical PI controller, (b) conventional IDA PBC, (c) proposed IDA PBC IA controller.

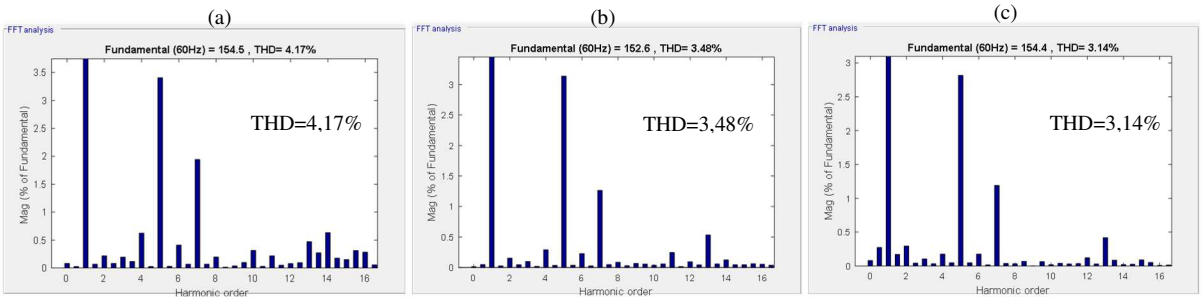

Fig. 13. Comparative experimental THD results in case of nonlinear load: (a) classical PI controller, (b) conventional IDA PBC, (c) proposed IDA PBC IA controller.

6.4. Dynamic tests based on simulation results

To verify the dynamic performances of the proposed control under additional constraining load conditions, the cases of nonlinear and inductive load steps are investigated. Simulation tests are performed under MATLAB/Simulink software. The obtained results are compared to those of a classical PI and a conventional IDA-PBC controller.

6.4.1. Nonlinear step load

In this test the used nonlinear loads are diode rectifiers feeding an R-C loads of 2 kW, where (R=35Ω and C=100µF). The grid forming inverter supplies:

- one diode rectifier until t=0.2 s.

- two diode rectifiers with the same parameters after t=0.2s.

The comparison simulation results are presented in Fig. 14. These results illustrate that the proposed control ensures the fast response and the less voltage drop than the conventional IDA-PBC and the classical PI controller at the transient time.

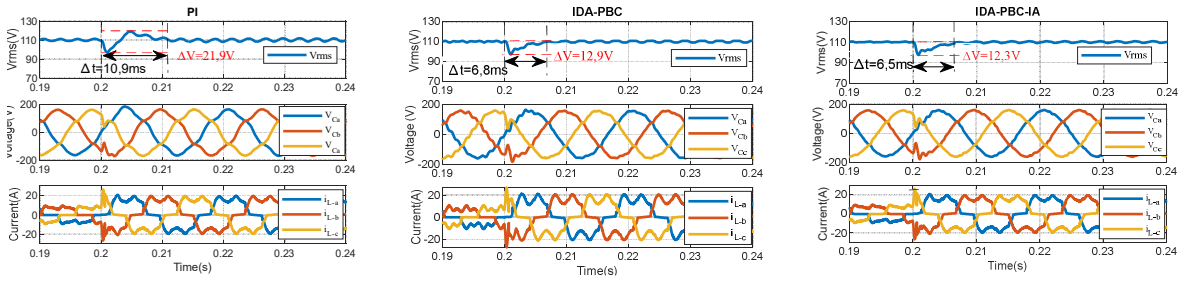

Fig. 14. Comparative simulation results showing the RMS voltage, the three-phase voltage and the load currents in case of a nonlinear load step change for respectively the classical PI controller, the conventional IDA-PBC and the proposed IDA-PBC-IA controller.

6.4.2. Inductive linear load

In this test, a step of 10 kVAR is performed at t=0.2 s. The used inductive load is a three-phase R-L branch (R=1Ω and L=9mH). Before the step, the supplied load is mostly resistive. The RMS voltage and the capacitor voltage V_{Ca} superimpose to the load current of the phase '*a*' are presented respectively for the PI, the IDA-PBC and the proposed IDA-PBC-IA

controller in the following Fig. 15. As it can be seen, the proposed control allows fast disturbance rejection compared to the PI controller and slight transition compared to the classical IDA-PBC controller.

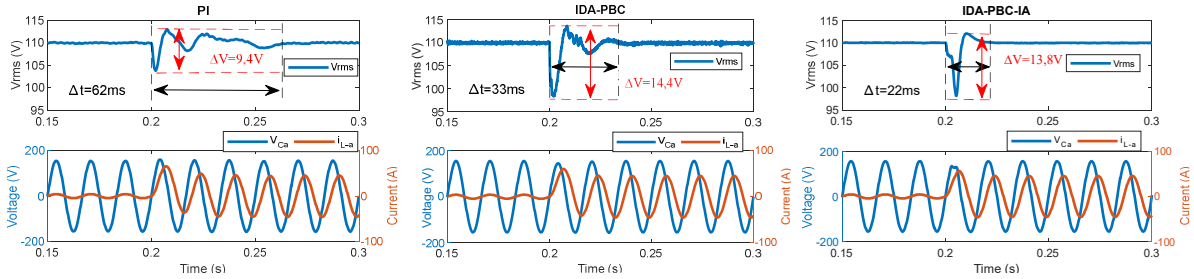

Fig. 15. Comparative simulation results showing the RMS voltage, the phase 'a' capacitor voltage V_{Ca} and the load current $i_{L\text{-}a}$ for a step inductive load (R=1Ω and L=9mH) for respectively the classical PI controller, the conventional IDA-PBC and the proposed IDA- PBC-IA controller

The measured voltage THD rates at the steady-state are about 0,34%, 0,26% and 0,19% for respectively the classical PI, the conventional IDA-PBC and the proposed IDA-PBC-IA. These THD rates are presented in Fig. 16 and highlight the performance of the proposed controller.

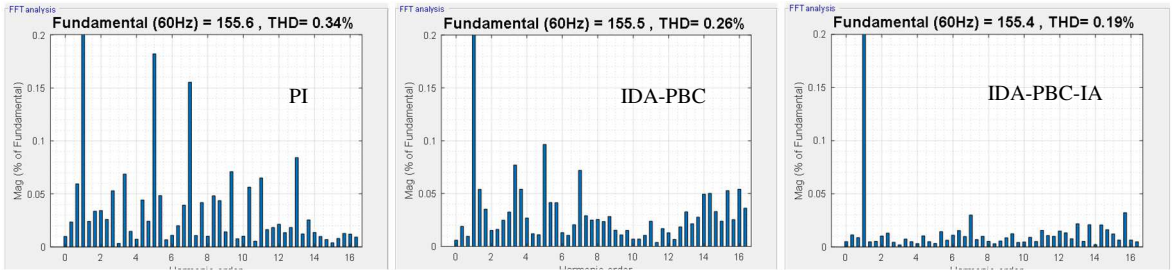

Fig. 16. Comparative THD results in case of linear inductive load for respectively the classical PI controller, the conventional IDA- PBC and the proposed IDA-PBC-IA controller

6.5. Discussion

To summarize the performances and the limits of the studied control techniques, the following TABLE VII presents the obtained controller performances for each control test.

TABLE VII. Comparative performances between the different controllers.

Tests	**Comparison**	**PI controller**	**IDA-PBC**	**IDA-PBC-IA**

		parameters		controller	controller
Linear load		THD	*1%*	*0.8%*	*0.7%*
Nonlinear load		THD	*4,17%*	*3,48%*	*3,14%*
Unbalance load condition		THD	*4,55%*	*2,62%*	*2,38%*
Dynamic test	Step load	Voltage drop	*36V*	*27V*	*12V*
	Start-up	Response time	*22,48ms*	*21,61ms*	*6,59ms*
Robustness test		Effectiveness	✓	✓✓	✓✓✓
Computation time		Time	*30,4µs*	*26,5µs*	*30,9µs*

Based on these results, we can say that the proposed controller (IDA-PBC-IA) presents high performances compared to the other studied control techniques. It allows having the short response time in front of linear step load, the less THD rate in the case of a linear load and the best effectiveness in case of occurrence of parametric variation. The same remark can be done in case of nonlinear load, where the obtained THD is very advantageous for the proposed control technique than for the rest of the used controllers. These results are expected, Indeed the proposed control allows by its structure that mix the advantages of the classical IDA-PBC controller to the advantages of the PI controller to synthesize a control law guaranteeing the stability of the closed-loop system while enhancing the robustness of the system and managing the problem of parameter uncertainty in both linear, nonlinear and under unbalanced load conditions.

These results are expected, Indeed the proposed control allows by its structure that incorporate the advantages of the classical IDA-PBC controller to synthesize a control law guaranteeing the stability of the closed-loop system to the advantages of the PI controller

allowing to enhance the robustness of the system and manage the problem of parameter uncertainty in both linear, nonlinear and under unbalanced load conditions.

Since this control technique is considered as the mixing of two control laws, this effect appears on the computation time measured by dSPACE. It can easily be seen that the execution time of the proposed control (30,9µs) is slightly higher than that of the two other controls (PI and classical IDA-PBC) which show respectively the execution time of 26,5µs and 30,4µs. This small excess on time is due to the presence of extra control loops compared to both PI and IDA–PBC.

Regarding the control synthesis technique where unlike the classical PI control in which the use of the pole placement technique allows the synthesis of the controller parameters, the classical and the proposed IDA–PBC-IA control difficulties are to keep the Hamiltonian form to synthesize the controller parameters. One more difficulty is encountered with the proposed one is when adding the integral action and increasing the order of the system while respecting also the Hamiltonian geometry. Indeed, the Hamiltonian structure imposes an accurate choice of parameters that should be verified to ensure a fast convergence of the system to the point of stable equilibrium. Theoretically, no method allows obtaining precise parameters choice for the proposed controller like that of pole placement method employed to get the PI controller parameters where the dynamic is fixed apriority. However, the parameters are selected by an empirical method using try and error observation to achieve a law voltage THD and ensure fast time response to get the best control performances.

7. Conclusion

In this paper, a robust IDA-PBC with an integral action strategy for voltage quality enhancement in isolated micro-grid is proposed. The main purpose of the proposed technique is to increase the robustness to a conventional IDA-PBC system by incorporating an integral action in which the Hamiltonian structure of the system is maintained. Thereby the closed-

loop stability is guaranteed while the robustness and disturbance rejection proprieties are enhanced. The system is modeled in Hamiltonian form, and then the steps to synthesize the proposed control are provided. Based on an experimental comparative study between a classical PI, a conventional IDA-PBC, and the proposed control IDA-PBC-IA, it is demonstrated that the proposed control can achieve better power quality either in linear, nonlinear, balanced and unbalanced load conditions.

References

[1] P. Sreekumar, V. Khadkikar, Adaptive Power Management Strategy for Effective Volt–Ampere Utilization of a Photovoltaic Generation Unit in Standalone Microgrids, IEEE Transactions on Industry Applications. 54 (2018) 1784–1792. doi:10.1109/TIA.2017.2781643.

[2] A. Eshraghi, R. Ghorbani, Islanding detection and over voltage mitigation using controllable loads, Sustainable Energy, Grids and Networks. 6 (2016) 125–135. doi:10.1016/j.segan.2016.02.007.

[3] P.C. Sahu, S. Mishra, R.C. Prusty, S. Panda, Improved-salp swarm optimized type-II fuzzy controller in load frequency control of multi area islanded AC microgrid, Sustainable Energy, Grids and Networks. 16 (2018) 380–392. doi:10.1016/j.segan.2018.10.003.

[4] A.H. Hubble, T.S. Ustun, Composition, placement, and economics of rural microgrids for ensuring sustainable development, Sustainable Energy, Grids and Networks. 13 (2018) 1–18. doi:10.1016/j.segan.2017.10.001.

[5] I.D.N. de Souza, P.M. de Almeida, P.G. Barbosa, C.A. Duque, P.F. Ribeiro, Digital single voltage loop control of a VSI with LC output filter, Sustainable Energy, Grids and Networks. 16 (2018) 145–155. doi:10.1016/j.segan.2018.07.004.

[6] N. Khefifi, A. Houari, M. Ait-Ahmed, M. Machmoum, M. Ghanes, Robust IDA-PBC Based Load Voltage Controller for Power Quality Enhancement of Standalone Microgrids, in: IECON 2018 - 44th Annual Conference of the IEEE Industrial Electronics Society, 2018: pp. 249–254. doi:10.1109/IECON.2018.8591805.

[7] M. Pichan, H. Rastegar, Sliding-Mode Control of Four-Leg Inverter With Fixed Switching Frequency for Uninterruptible Power Supply Applications, IEEE Transactions on Industrial Electronics. 64 (2017) 6805–6814. doi:10.1109/TIE.2017.2686346.

[8] S. Khalid, B. Dwivedi, Power quality issues, problems, standards & their effects in industry with corrective means, International Journal of Advances in Engineering & Technology ©IJAET ISSN. 1 (2011) 2231–19631.

[9] M. Shahparasti, M. Mohamadian, A. Yazdian, A.A. Ahmad, M. Amini, Derivation of a Stationary-Frame Single-Loop Controller for Three-Phase Standalone Inverter Supplying Nonlinear Loads, IEEE Transactions on Power Electronics. 29 (2014) 5063–5071. doi:10.1109/TPEL.2013.2287906.

[10] P.C. Loh, M.J. Newman, D.N. Zmood, D.G. Holmes, A comparative analysis of multiloop voltage regulation strategies for single and three-phase UPS systems, IEEE Transactions on Power Electronics. 18 (2003) 1176–1185. doi:10.1109/TPEL.2003.816199.

[11] S.J. Williamson, A. Griffo, B.H. Stark, J.D. Booker, A controller for single-phase parallel inverters in a variable-head pico-hydropower off-grid network, Sustainable Energy, Grids and Networks. 5 (2016) 114–124. doi:10.1016/j.segan.2015.11.006.

[12] Z. Li, C. Zang, P. Zeng, H. Yu, S. Li, J. Bian, Control of a Grid-Forming Inverter Based on Sliding-Mode and Mixed $H_2/H_ınfty $ Control, IEEE Transactions on Industrial Electronics. 64 (2017) 3862–3872. doi:10.1109/TIE.2016.2636798.

[13] D. Pullaguram, S. Mishra, N. Senroy, M. Mukherjee, Design and Tuning of Robust Fractional Order Controller for Autonomous Microgrid VSC System, IEEE Transactions on Industry Applications. 54 (2018) 91–101. doi:10.1109/TIA.2017.2758755.

[14] S. Dhar, P.K. Dash, Adaptive backstepping sliding mode control of a grid interactive PV-VSC system with LCL filter, Sustainable Energy, Grids and Networks. 6 (2016) 109–124. doi:10.1016/j.segan.2016.03.001.

[15] W. Lu, K. Zhou, D. Wang, M. Cheng, A General Parallel Structure Repetitive Control Scheme for Multiphase DC–AC PWM Converters, IEEE Transactions on Power Electronics. 28 (2013) 3980–3987. doi:10.1109/TPEL.2012.2229395.

[16] S. Jiang, D. Cao, Y. Li, J. Liu, F.Z. Peng, Low-THD, Fast-Transient, and Cost-Effective Synchronous-Frame Repetitive Controller for Three-Phase UPS Inverters, IEEE Transactions on Power Electronics. 27 (2012) 2994–3005. doi:10.1109/TPEL.2011.2178266.

[17] H.-K. Kang, C.-H. Yoo, I.-Y. Chung, D.-J. Won, S.-I. Moon, Intelligent Coordination Method of Multiple Distributed Resources for Harmonic Current Compensation in a Microgrid, Journal of Electrical Engineering and Technology. 7 (2012) 834–844. doi:10.5370/JEET.2012.7.6.834.

[18] H.T. Nguyen, E. Kim, I. Kim, H.H. Choi, J. Jung, Model Predictive Control with Modulated Optimal Vector for a Three-Phase Inverter with an LC Filter, IEEE Transactions on Power Electronics. 33 (2018) 2690–2703. doi:10.1109/TPEL.2017.2694049.

[19] S. Bayhan, M. Trabelsi, H. Abu-Rub, M. Malinowski, Finite-Control-Set Model-Predictive Control for a Quasi-Z-Source Four-Leg Inverter Under Unbalanced Load Condition, IEEE Transactions on Industrial Electronics. 64 (2017) 2560–2569. doi:10.1109/TIE.2016.2632062.

[20] S. Mohagheghi, Y. del Valle, G.K. Venayagamoorthy, R.G. Harley, A Proportional-Integrator Type Adaptive Critic Design-Based Neurocontroller for a Static Compensator in a Multimachine Power System, IEEE Transactions on Industrial Electronics. 54 (2007) 86–96. doi:10.1109/TIE.2006.888760.

[21] Y. Naderi, S.H. Hosseini, S.G. Zadeh, B. Mohammadi-Ivatloo, M. Savaghebi, J.M. Guerrero, An optimized direct control method applied to multilevel inverter for microgrid power quality enhancement, International Journal of Electrical Power & Energy Systems. 107 (2019) 496–506. doi:10.1016/j.ijepes.2018.12.007.

[22] D. Heredero-Peris, C. Chillón-Antón, E. Sánchez-Sánchez, D. Montesinos-Miracle, Fractional proportional-resonant current controllers for voltage source converters, Electric Power Systems Research. 168 (2019) 20–45. doi:10.1016/j.epsr.2018.09.014.

[23] D. Çelík, M.E. Meral, A flexible control strategy with overcurrent limitation in distributed generation systems, International Journal of Electrical Power & Energy Systems. 104 (2019) 456–471. doi:10.1016/j.ijepes.2018.06.048.

[24] D. Kim, D. Lee, Feedback Linearization Control of Three-Phase UPS Inverter Systems, IEEE Transactions on Industrial Electronics. 57 (2010) 963–968. doi:10.1109/TIE.2009.2038404.

[25] G. Lou, W. Gu, W. Sheng, X. Song, F. Gao, Distributed Model Predictive Secondary Voltage Control of Islanded Microgrids With Feedback Linearization, IEEE Access. 6 (2018) 50169–50178. doi:10.1109/ACCESS.2018.2869280.

[26] R. Wai, C. Lin, W. Wu, H. Huang, Design of backstepping control for high-performance inverter with stand-alone and grid-connected power-supply modes, IET Power Electronics. 6 (2013) 752–762. doi:10.1049/iet-pel.2012.0579.

[27] H. Huerta, A.G. Loukianov, J.M. Cañedo, Passivity Sliding Mode Control of Large-Scale Power Systems, IEEE Transactions on Control Systems Technology. (2018) 1–9. doi:10.1109/TCST.2018.2791928.

[28] A. Houari, A. Djerioui, A. Saim, M. Ait-Ahmed, M. Machmoum, Improved control strategy for power quality enhancement in standalone systems based on four-leg voltage source inverters, IET Power Electronics. 11 (2018) 515–523. doi:10.1049/iet-pel.2017.0124.

[29] F. Yazdi, S.H. Hosseinian, A novel "Smart Branch" for power quality improvement in microgrids, International Journal of Electrical Power & Energy Systems. 110 (2019) 161–170. doi:10.1016/j.ijepes.2019.02.026.

[30] M. Monfared, H. Rastegar, Design and experimental verification of a dead beat power control strategy for low cost three phase PWM converters, International Journal of Electrical Power & Energy Systems. 42 (2012) 418–425. doi:10.1016/j.ijepes.2012.04.044.

[31] J.S. Lim, C. Park, J. Han, Y.I. Lee, Robust Tracking Control of a Three-Phase DC–AC Inverter for UPS Applications, IEEE Transactions on Industrial Electronics. 61 (2014) 4142–4151. doi:10.1109/TIE.2013.2284155.

[32] H. Heydari-doostabad, R. Ghazi, A new approach to design an observer for load current of UPS based on Fourier series theory in model predictive control system, International Journal of Electrical Power & Energy Systems. 104 (2019) 898–909. doi:10.1016/j.ijepes.2018.07.047.

[33] P. Cortes, G. Ortiz, J.I. Yuz, J. Rodriguez, S. Vazquez, L.G. Franquelo, Model Predictive Control of an Inverter With OutputLCFilter for UPS Applications, IEEE Transactions on Industrial Electronics. 56 (2009) 1875–1883. doi:10.1109/TIE.2009.2015750.

[34] H.A. Young, M.A. Perez, J. Rodriguez, H. Abu-Rub, Assessing Finite-Control-Set Model Predictive Control: A Comparison with a Linear Current Controller in Two-Level Voltage Source Inverters, IEEE Industrial Electronics Magazine. 8 (2014) 44–52. doi:10.1109/MIE.2013.2294870.

[35] R. Ortega, A. van der Schaft, F. Castanos, A. Astolfi, A. Astolfi, Control by Interconnection and Standard Passivity-Based Control of Port-Hamiltonian Systems, IEEE Transactions on Automatic Control. 53 (2008) 2527–2542. doi:10.1109/TAC.2008.2006930.

[36] O.D. Montoya, A. Garcés, G. Espinosa-Pérez, A generalized passivity-based control approach for power compensation in distribution systems using electrical energy storage systems, Journal of Energy Storage. 16 (2018) 259–268. doi:10.1016/j.est.2018.01.018.

[37] B. Yang, T. Yu, H. Shu, Y. Zhang, J. Chen, Y. Sang, L. Jiang, Passivity-based sliding-mode control design for optimal power extraction of a PMSG based variable speed wind turbine, Renewable Energy. 119 (2018) 577–589. doi:10.1016/j.renene.2017.12.047.

[38] O.D. Montoya, W. Gil-González, F.M. Serra, PBC Approach for SMES Devices in Electric Distribution Networks, IEEE Transactions on Circuits and Systems II: Express Briefs. 65 (2018) 2003–2007. doi:10.1109/TCSII.2018.2805774.

[39] F.M. Serra, C.H. De Angelo, IDA-PBC controller design for grid connected Front End Converters under non-ideal grid conditions, Electric Power Systems Research. 142 (2017) 12–19. doi:10.1016/j.epsr.2016.08.041.

[40] S. Sanchez, R. Ortega, R. Griño, G. Bergna, M. Molinas, Conditions for Existence of Equilibria of Systems With Constant Power Loads, IEEE Transactions on Circuits and Systems I: Regular Papers. 61 (2014) 2204–2211. doi:10.1109/TCSI.2013.2295953.

[41] R. Ortega, J.G. Romero, Robust integral control of port-Hamiltonian systems: The case of non-passive outputs with unmatched disturbances, Systems & Control Letters. 61 (2012) 11–17. doi:10.1016/j.sysconle.2011.09.015.

[42] R.V. Meshram, M. Bhagwat, S. Khade, S.R. Wagh, A.M. Stanković, N.M. Singh, Port-Controlled Phasor Hamiltonian Modeling and IDA-PBC Control of Solid-State Transformer, IEEE Transactions on Control Systems Technology. 27 (2019) 161–174. doi:10.1109/TCST.2017.2761866.

[43] M. Hilairet, M. Ghanes, O. Béthoux, V. Tanasa, J.-P. Barbot, D. Normand-Cyrot, A passivity-based controller for coordination of converters in a fuel cell system, Control Engineering Practice. 21 (2013) 1097–1109. doi:10.1016/j.conengprac.2013.04.003.

[44] A. Donaire, S. Junco, On the addition of integral action to port-controlled Hamiltonian systems, Automatica. 45 (2009) 1910–1916. doi:10.1016/j.automatica.2009.04.006.